Scientific Research Publishing

World Journal of Mechanics, 2026, 16(2), 31-51
https://www.scirp.org/journal/wjm
ISSN Online: 2160-0503
ISSN Print: 2160-049X

Strongly Nonlinear Effects of an Unbalanced Mass and the Supply Voltage of the Non-Ideal DC Motor on the Vibration Amplitude of a Thin Rectangular Plate

Lionel Merveil Anague Tabejieu[1,2*], Cabrel Fotso Kamche[1], Vanlie Maurice Kontchou[3], Eric Sinclair Fongho[1], Joseph Nkongho Anyi[1,4]

[1]Laboratory of Mechanics and Materials, Department of Mechanical Engineering, National Higher Polytechnic, School of Douala, University of Douala, Douala, Cameroon
[2]Laboratory of Modelling and Simulation in Engineering, Biomimetics and Prototypes and TWAS Research Unit, Faculty of Science, University of Yaoundé I, Yaoundé, Cameroon
[3]Department of Maritime and Port Engineering, National Higher Polytechnic, School of Douala, University of Douala, Douala, Cameroon
[4]Department of Mechanical Engineering, Higher Technical Teachers Training, College of Kumba of the University of Buea in Kumba, Kumba, Cameroon
Email: *lmanaguetabejieu@gmail.com

How to cite this paper: Anague Tabejieu, L.M., Kamche, C.F., Kontchou, V.M., Fongho, E.S. and Anyi, J.N. (2026) Strongly Nonlinear Effects of an Unbalanced Mass and the Supply Voltage of the Non-Ideal DC Motor on the Vibration Amplitude of a Thin Rectangular Plate. *World Journal of Mechanics*, **16**, 31-51.
https://doi.org/10.4236/wjm.2026.162002

Received: January 5, 2026
Accepted: February 24, 2026
Published: February 27, 2026

Abstract

In this paper, the strongly nonlinear effects of an unbalanced mass and the supply voltage of a non-ideal DC motor on the vibration amplitude of a thin rectangular plate are investigated. The influence of these two parameters on the occurrence of the Sommerfeld phenomenon—specifically in terms of the energy delivered by the motor—as well as on the emergence of the so-called limited energy source phenomenon related to voltage saturation, is thoroughly analyzed using analytical and numerical methods. By considering the interaction between the thin rectangular plate and the non-ideal DC motor, the governing equations of the vibration system are derived using the Lagrange formalism. A perturbation method based on averaging is then employed to obtain the steady-state response. Numerical simulations using the fourth-order Runge–Kutta method are also conducted to validate the analytical results. The effect of the non-ideal loading is strongly nonlinear, leading to a non-monotonic behavior of the vibration amplitude with respect to both the supply voltage and the unbalanced mass of the motor. Moreover, the amplitude jump phenomenon, which indicates the presence of the Sommerfeld effect, is clearly captured across a wide range of parameters. This paper provides useful insights for the design of industrial floor structures that support rotating ma-

chinery.

Keywords

Unbalanced Mass, Non-Ideal DC Motors, Sommerfeld Effect, Thin Rectangular Plate, Amplitude of Vibration, Supply Voltage

1. Introduction

The dynamic behaviour of plate structures is governed by the nature of the loading. It can be influenced by natural or artificial forces such as wind, earthquakes, explosions, and even vibrations from electric motors. Plate structures are widely used in mechanical and civil engineering. They are employed in the construction of infrastructures such as boats, airplanes, rockets, satellites, tunnels, bridges, and buildings. In this work, we study the behaviour of a plate subjected to vibrations from an electric motor. Structures experiencing such vibrations are referred to in the literature as non-ideal systems. It should be noted that the study of such systems dates back hundreds of years, as the very first type of non-ideal system was created in 1889. However, it was not until 1902 that this type of system appeared in the scientific literature [1]. A plate structure under non-ideal loading exhibits an interaction between the motor and the plate [2]. When the energy provided by the non-ideal motor is insufficient to drive the system through the resonance region, a nonlinear jump phenomenon, known as the Sommerfeld effect, may occur near the natural frequency [3]. In recent years, many authors have investigated the Sommerfeld effect in non-ideal systems. Jorge and Balthazar studied the nonlinear dynamics of a non-ideal Duffing-Rayleigh oscillator. They found that for a nonlinear stiffness and nonlinear damping beam, the Sommerfeld effect may be observed [4]. Balthazar *et al.* [5] presented the appearance of the Sommerfeld effect in the evolution of vibration amplitude and observed the influence of the damping coefficient on this effect. Kovriguine [6] analyzed a classical problem of an oscillator on an elastic base caused by rotor vibrations of an asynchronous driver near the critical angular velocity. Kong and Jiang [7] studied the Sommerfeld effect and the synchronization of two motors mounted on a simply supported beam, showing that structural parameters influence the appearance of the Sommerfeld effect. Li *et al.* [8] studied the nonlinear dynamic response of a thin rectangular plate vibration system excited by a non-ideal induction motor. They derived the equations for the plate structure under non-ideal vibration and noted the occurrence of the Sommerfeld effect. Kong *et al.* [9] worked on the dynamic stability of thin rectangular plates subjected to excitations from three vibrators, discussing the effects of unbalanced masses and installation positions of the vibrators on self-synchronization behaviour, the Sommerfeld effect, and the dynamic response of the system. Paulo Gonçalves *et al.* [10] analyzed a cantilever beam with a non-ideal DC motor installed at the free end and found that the Sommer-

feld effect was related to certain system parameters.

Despite these advances, the analysis of the vibration amplitude response of a thin rectangular plate structure subjected to a non-ideal DC motor remains insufficiently explored. Specifically, the effects of the unbalanced mass and the supply voltage on the occurrence of nonlinear phenomena such as the Sommerfeld effect—in terms of the energy delivered by the motor—as well as on the appearance of the so-called limited energy source phenomenon related to voltage saturation, which considerably affects the system response, have yet to be fully addressed. This study aims to fill this gap. A rigorous formulation of the DC motor–plate interaction is established, and an analytical development is proposed. The effect of the non-ideal loading, which is highly nonlinear, is analyzed, leading to a non-monotonic behaviour of the plate amplitude with respect to both the supply voltage and the unbalanced mass of the motor. Finally, the amplitude jump phenomenon, indicating the presence of the Sommerfeld effect, is correctly captured by the analysis across a wide range of parameters.

The remainder of the paper is organized as follows. **Section 2** presents the physical description of the system and its mathematical modelling. **Section 3** explores the influence of the unbalanced mass, the supply voltage, and the plate damping coefficient on system stability. The conclusion is given in **Section 4**.

2. Mathematical Modeling of the System

2.1. Description of the System

The system consists of a thin rectangular plate of length a, width b, and thickness h, with two opposite edges simply supported and the other two edges free. A DC motor carrying an unbalanced mass is mounted on the plate. The contact surface between the motor and the plate is taken into account through the area A_c. A schematic of the setup is shown in **Figure 1**. This system can be considered analogous to an industrial floor supporting rotating machinery.

The angular displacement of the motor shaft is denoted by θ. The rotor has a moment of inertia J and carries an unbalanced mass m_0 located at a distance d from the axis. The characteristic driving torque of the motor for a given energy level is assumed to be known, either from the manufacturer or from experiments.

2.2. Mathematical Formalism

In order to derive the equations of motion, the following assumptions are made:

1) the rectangular plate is thin $\left(h \ll \min(a,b)\right)$ and $\left(h/\min(a,b) \prec 0.1\right)$ [11];

2) the plate is assumed to behave according to the Kirchhoff's hypothesis [11] [12];

3) only the transverse vibration of the thin plate is considered, while displacements in the x-axis and y-axis directions are neglected;

4) variations of cross-sectional dimensions are negligible;

5) the contact surface between the DC motor and the plate is rigid.

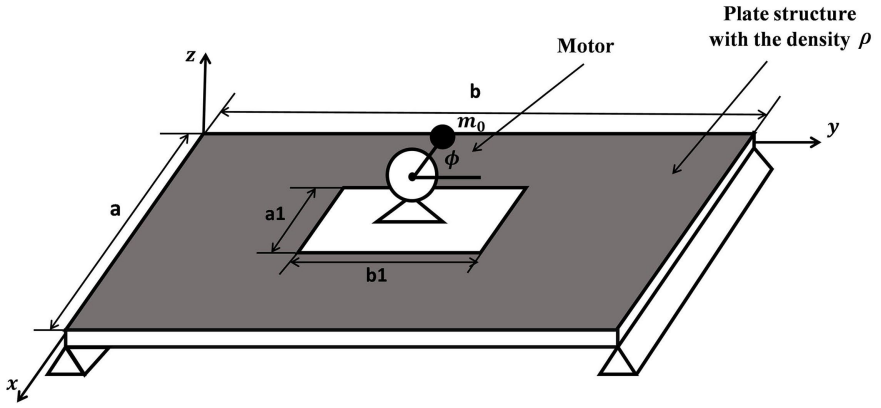

Figure 1. The general plan of the analyzed thin rectangular plate supporting a non-ideal DC motor.

To obtain the dynamic equations of the system, we combine the kinetic energies of the plate and the motor. Let T be the total kinetic energy of the system. It follows that:

$$T = T_{plate} + T_{motor} \tag{1}$$

where the kinetic energy of the plate, T_{plate}, and that of the non-ideal DC motor, T_{motor}, as follows (according to the assumptions listed above) [11]-[13]:

$$\begin{cases} T_{plate} = \dfrac{1}{2}\rho h \displaystyle\int_S \left(\frac{\partial w}{\partial t}\right)^2 \mathrm{d}S \\ T_{motor} = \dfrac{1}{2}J\left(\dfrac{\partial \phi}{\partial t}\right)^2 + \dfrac{1}{2a_1 b_1} m_0 \displaystyle\int_S \left(\left(\frac{\partial w}{\partial t}\right)^2 + 2d\frac{\partial w}{\partial t}\frac{\partial \phi}{\partial t}\cos(\varphi) + d^2\left(\frac{\partial \phi}{\partial t}\right)^2\right) \\ \qquad \times\left[H(x-x_0) - H(x-x_0')\right]\times\left[H(y-y_0) - H(y-y_0')\right]\mathrm{d}S \end{cases} \tag{2}$$

where ρ is the density of the plate material, and $w(x,y,t)$ is the transverse displacement of the plate. H represents the Heaviside function, defined as follows:

$$H(x) = \begin{cases} 0 & \text{if } x \prec 0 \\ 1 & \text{if } x \prec 0 \end{cases} \tag{3}$$

Here, $a_1 = x_0' - x_0$ and $b_1 = y_0' - y_0$ stand for the dimensions occupied by the motor on the plate along the x- and y-axes, respectively, with x_0', x_0, y_0' and y_0 denoting the coordinates of the boundaries of the areas occupied by the DC motor, in the x and y directions, respectively.

On the other hand, the total potential energy of the system is derived as follows:

$$V = V_{plate} + V_{motor} \tag{4}$$

where the potential energy of the plate, V_{plate}, and that of the non-ideal DC motors, V_{motor}, are expressed as (according to the assumptions listed previously) [11]-[13]:

$$\begin{cases} V_{plate} = \dfrac{h^3}{12}\left(\displaystyle\int_S \frac{\lambda}{2}\left(\frac{\partial^2 w}{\partial x^2} + \frac{\partial^2 w}{\partial y^2}\right)^2 + D\left(\left(\frac{\partial^2 w}{\partial x^2}\right)^2 + \left(\frac{\partial^2 w}{\partial y^2}\right)^2 + 2\left(\frac{\partial^2 w}{\partial x \partial y}\right)^2\right)\mathrm{d}S\right)\mathrm{d}S \\ V_{motor} = m_0 g\left(d\sin(\phi)\right) \end{cases} \tag{5}$$

The energy of the external force W and the dissipation function D_0 of the system are expressed as follows:

$$W=\left(T_m-u_0\dot{\phi}\right)\phi;\quad D_0=\frac{1}{2}\lambda h\int_S\left(\frac{\partial w}{\partial t}\right)^2\mathrm{d}S \tag{6}$$

where T_m, u_0 and λ are respectively the electromechanical torque, the viscous friction coefficient associated with the slipping of parts in the motor, and the damping coefficient of the plate. Having the expressions of the total energies of the system, we define the Lagrangian function [14] and obtain the resulting equations of motion for the non-ideal system shown in **Figure 1** as follows:

$$\begin{aligned}&\left(\rho h+\frac{m_0}{ab}\right)\frac{\partial^2 w}{\partial t^2}+\lambda h\frac{\partial w}{\partial t}+D\left(\frac{\partial^4 w}{\partial x^4}+\frac{\partial^4 w}{\partial y^4}+2\frac{\partial^4 w}{\partial x^2\partial y^2}\right)\\&=\frac{dm_0}{a_1b_1}\left(\left(\frac{\partial\phi}{\partial t}\right)^2\sin(\phi)-\frac{\partial^2\phi}{\partial t^2}\cos(\phi)\right)\left[H(x-x_0)-H(x-x_0')\right]\\&\times\left[H(y-y_0)-H(y-y_0')\right]\end{aligned} \tag{7a}$$

$$\left(J+m_0d^2\right)\frac{\partial^2\phi}{\partial t^2}+u_0\dot{\phi}+\frac{m_0d}{2}\frac{\partial^2 w}{\partial t^2}\cos(\phi)+m_0gd\cos(\phi)=T_m \tag{7b}$$

According to [15], the electromechanical torque is evaluated (after modelled the DC motor as an electromechanical system) as:

$$T_m=\frac{K_b}{R_a}\left(U_a-K_b\omega_m\right) \tag{8}$$

R_a is the motor winding resistance, U_a the supply voltage of the motor, K_b is the back-emf constant and ω_m is the angular velocity of the motor shaft. In the configuration shown in **Figure 1**, the plate has two opposite simply supported edges, while the other two are free. The boundary conditions of the simply supported edges (zero transverse displacement and zero flexural moments) [16] are:

$$\text{at}\quad y=0;y=b\quad\begin{cases}w(x,0,t)=0;\quad w(x,b,t)=0\\\dfrac{\partial^2 w}{\partial y^2}(x,0,t)=0;\quad\dfrac{\partial^2 w}{\partial y^2}(x,b,t)=0\end{cases} \tag{9}$$

The boundary conditions for the free edges (zero flexural and zero torsional moments) are: [16] are:

$$\text{at}\quad x=0;x=a:\begin{cases}M_x=\dfrac{\partial^2 w}{\partial x^2}(0,y,t)=0;M_x=\dfrac{\partial^2 w}{\partial x^2}(a,y,t)=0\\M_{xy}=\dfrac{\partial^2 w}{\partial x\partial y}(0,y,t)=0;M_{xy}=\dfrac{\partial^2 w}{\partial x\partial y}(a,y,t)=0\end{cases} \tag{10}$$

To investigate the amplitude response of the system let us derive the modal equations. To do so, Galerkin's method is applied [17] [18]. According to this method, the solution of the partial differential **Equation (7a)** and **Equation (7b)** is assumed to be of the form:

$$w(x,y,t)=\sum_{n=1}^{\infty}\sum_{m=1}^{\infty}q_{nm}(t)\varphi_{nm}(x,y) \tag{11}$$

where $q_{nm}(t)$ is the generalized coordinates, $\varphi_{nm}(x,y)$ is the assumed mode shape function that depends on the boundary conditions of the free oscillations of the plate and (n, m) denotes the natural mode with n and m nodal lines lying the x and y directions, respectively. To apply the method, **Equations (8)-(11)** are substituted into **Equation (7a)** and **Equation (7b)**. The resulting equation is then multiplied by the corresponding eigenfunction and integrated over the surface area of the plate. After some algebraic manipulations, the modal equation is obtained as follows:

$$\begin{aligned} &M_{nm}\ddot{q}_{nm}(t)+\lambda_{nm}\dot{q}_{nm}(t)+K_{nm}q_{nm}(t)\\ &=\frac{d\,m_0}{a_1b_1}\left(\left(\dot{\phi}\right)^2\sin(\phi)-\ddot{\phi}\cos(\phi)\right)f_{nm} \end{aligned} \tag{12a}$$

$$\begin{aligned} &\left(J+m_0\,d^2\right)\ddot{\phi}+\left(u_0+\frac{K_b^2}{R_a}\right)\dot{\phi}+\left(\frac{L_{nm}}{2T_{nm}}\right)m_0\,d\,\ddot{q}_{nm}(t)\cos(\phi)\\ &+m_0\,g\,d\cos(\phi)=\frac{K_b}{R_a}U_a \end{aligned} \tag{12b}$$

with:

$$\begin{aligned} &M_{nm}=\left(\rho h+\frac{m_0}{ab}\right)\int_0^a\int_0^b\varphi_{nm}^2(x,y)\,\mathrm{d}x\,\mathrm{d}y;\ \lambda_{nm}=\lambda h\int_0^a\int_0^b\varphi_{nm}^2(x,y)\,\mathrm{d}x\,\mathrm{d}y;\\ &K_{nm}=D\int_0^a\int_0^b\varphi_{nm}(x,y)\left(\frac{\partial^4\varphi_{nm}(x,y)}{\partial x^4}+\frac{\partial^4\varphi_{nm}(x,y)}{\partial y^4}+2\frac{\partial^4\varphi_{nm}(x,y)}{\partial x^2\partial y^2}\right)\mathrm{d}x\,\mathrm{d}y;\\ &f_{nm}=\int_0^a\int_0^b\varphi_{nm}(x,y)\left[H(x-x_0)-H(x-x_0')\right]\times\left[H(y-y_0)-H(y-y_0')\right]\mathrm{d}x\,\mathrm{d}y;\\ &T_{nm}=\int_0^a\int_0^b\varphi_{nm}(x,y)\,\mathrm{d}x\,\mathrm{d}y;\ L_{nm}=\int_0^a\int_0^b\varphi_{nm}^2(x,y)\,\mathrm{d}x\,\mathrm{d}y. \end{aligned} \tag{13}$$

According to the boundary conditions **Equation (9)** and **Equation (10)**, the mode shape function and the natural frequency of the plate vibration are derived in **Appendix 1** and are given by

$$\begin{aligned} &\varphi_{nm}(x,y)\\ &=\left(\frac{ch(\tau_n a)-\cos(\alpha_n a)}{\sin(\alpha_n a)+\frac{\tau_n}{\alpha_n}sh(\tau_n a)}\left(\sin(\alpha_n x)-\frac{\alpha_n}{\tau_n}sh(\tau_n x)\right)+\cos(\alpha_n x)+\left(\frac{\alpha_n}{\tau_n}\right)^2ch(\tau_n x)\right)\sin\left(\frac{m\pi y}{b}\right) \end{aligned}$$

$$\omega_{nm}=\left(\frac{\alpha_n^2+\tau_n^2}{2}\right)\sqrt{\frac{D}{\rho h}} \tag{14}$$

where α_n and τ_n satisfy the following transcendental equation for the natural frequency (see **Appendix 1**):

$$\left(\alpha_n^2-\tau_n^2\right)sh(\tau_n a)\sin(\alpha_n a)+2\alpha_n\tau_n\left(ch(\tau_n a)\cos(\alpha_n a)-1\right)=0 \tag{15}$$

By substituting **Equation (14)** and **Equation (15)** into **Equation (13)**, all integrals are evaluated as shown in **Appendix 2**. To improve the accuracy of the nu-

merical calculations, the following dimensionless variables are defined:

$$y_{nm}(t)=\frac{q_{nm}(t)}{100\,d},\quad \tau=\omega_{nm}\,t \tag{16}$$

Equation (12a) and **Equation (12b)** then take the form:

$$\ddot{y}_{nm}+s\dot{y}_{nm}+\omega_0^2 y_{nm}=\varepsilon\left(\left(\dot{\phi}\right)^2\sin(\phi)-\ddot{\phi}\cos(\phi)\right) \tag{17a}$$

$$\ddot{\phi}+u_2^0\,\dot{\phi}+r\,\ddot{y}_{nm}\cos(\phi)+\alpha\cos(\phi)=u_1 \tag{17b}$$

$$\begin{gathered}s=\frac{\lambda_{nm}}{\sqrt{K_{nm}M_{nm}}};\ u_2^0=\frac{\left(u_0+\dfrac{K_b^2}{R_a}\right)}{\omega_{nm}\left(J+m_0\,d^2\right)};\quad \varepsilon=\frac{m_r f_{nm}}{100a_1b_1}\\ \alpha=\frac{m_0 gd}{\omega_{nm}^2\left(J+m_0d^2\right)};\quad u_1=\frac{U_a K_b}{R_a\,\omega_{nm}^2\left(J+m_0d^2\right)}\\ \omega_0^2=\frac{K_{nm}}{M_{nm}}\omega_{nm}^2;\ r=\frac{50L_{nm}m_0d^2}{\left(J+m_0d^2\right)T_{nm}};m_r=\frac{m_0}{M_{nm}}\end{gathered} \tag{18}$$

3. Dynamical Analysis

In this section, particular attention is focused on the analytical and numerical analysis of the effects of an unbalanced mass and the supply voltage of a non-ideal DC motor on the vibration amplitude of a thin rectangular plate.

3.1. Approximate Analytical Solution

We begin by using the averaging method [8] [19], which provides an analytical approximate solution and thus enables the detection of the main parameters' effects on the system response. Let us assume that the motor is operating in a steady state, so that the angular velocity and the supply voltage are constant (*i.e.*, $\ddot{\phi}=0$; $\dot{\phi}=\Omega\Rightarrow\phi=\Omega t$) [8]. By applying the averaging method to **Equation (17a)** and **Equation (17b)**, and averaging over the period $T=2\pi$, we obtain:

$$\ddot{y}_{nm}+s\,\dot{y}_{nm}+\omega_0^2\,y_{nm}=\varepsilon\Omega^2\sin(\Omega\tau) \tag{19a}$$

$$\frac{1}{2\pi}\int_0^{2\pi}u_2^0\,\dot{\phi}\,\mathrm{d}\phi+\frac{r}{2\pi}\int_0^{2\pi}\ddot{y}_{nm}\cos(\phi)\,\mathrm{d}\phi+\frac{\alpha}{2\pi}\int_0^{2\pi}\cos(\phi)\,\mathrm{d}\phi=u_1 \tag{19b}$$

The steady-state solution of **Equation (19a)** is obtained using the harmonic balance method [8] [19]

$$y_{nm}(\tau)=\frac{\varepsilon\Omega^2}{\sqrt{\left(\omega_0^2-\Omega^2\right)^2+(s\Omega)^2}}\sin\left(\Omega\tau-\arctan\left(\frac{s\Omega}{\omega_0^2-\Omega^2}\right)\right) \tag{20}$$

Substituting **Equation (20)** into **Equation (19b)**, yields:

$$u_2^0\,\Omega+\frac{r\varepsilon\Omega^5 s}{2\left(\left(\omega_0^2-\Omega^2\right)^2+(s\Omega)^2\right)}=u_1 \tag{21}$$

Equation (20) represents the steady-state response of the plate under DC motor, and **Equation (21)** is the steady-state response of the DC motor under vibration of the plate. Clearly, **Equation (21)** is a higher-order nonlinear transcendental equation, and obtaining its analytical solution is difficult.

The value of the average angular velocity Ω can be obtained numerically.

The average load torque is given by:

$$T_m = \frac{u_0}{\omega_{nm}\left(J + m_0 d^2\right)}\Omega + \frac{\varepsilon r \Omega^5 s}{2\left(\left(\omega_0^2 - \Omega^2\right)^2 + \left(s\,\Omega\right)^2\right)} \tag{22}$$

This equation reveals a nonlinear relationship between the average angular velocity, the unbalanced mass load, and the average load torque.

3.2. Approximate Numerical Solution

The physical and geometrical properties of the plate are listed in **Table 1** [8], and the parameters of the DC motor are listed in **Table 2** [8]. Accordingly, the dimensionless parameters given in **Equation (18)** are calculated.

In order to verify the precision of the analytical solution, we first solve the coupled **Equations (19a)-(21)** numerically using the fourth-order Runge-Kutta method [18] and the Dichotomy method [19]. The time step $\Delta\tau$ here used is $\Delta\tau = 0.01$, and the results are averaged over 10000 realizations. The initials conditions used are: $y_{nm}(0) = \dot{y}_{nm}(0) = 0$. Second, we present in several figures the effects of the main parameters (mode of vibration, unbalanced mass, and supply voltage of the DC motor) on the proposed model.

Table 1. Parameters of the thin rectangular plate [8].

Parameters	*Symbols*	*Values*
length (m)	b	1
Width (m)	a	0.5
thickness (m)	h	0.005
Young's modulus (N/m^2)	E	20.5×10^{10}
Poisson's ratio	μ	0.3
Density (kg/m^3)	ρ	7800
Length of the motor-plate' surface (m)	a_1	0.4
width of the motor-plate' surface (m)	b_1	0.2

Table 2. Parameters of the DC motor model [8].

Parameters	*Symbols*	*Values*
Friction coefficient (N·m·s/Rad)	u_0	1.67
Motor Constance (m/s)	k_b	2
Motor armature resistance (Ω)	R_b	0.5
Eccentric radius (m)	d	0.1
Moment of inertia J (kg·m^2)	J	0.015

In Figure 2 and Figure 3, the mode shapes obtained using **Equation (14)** and **Equation (15)** are reported. In Figure 2, we observe a single vibrating belly in the y-direction and no vibrating belly in the *x*-direction. In Figure 3, there are two vibrating bellies in the *y*-direction and no vibrating belly in the *x*-direction.

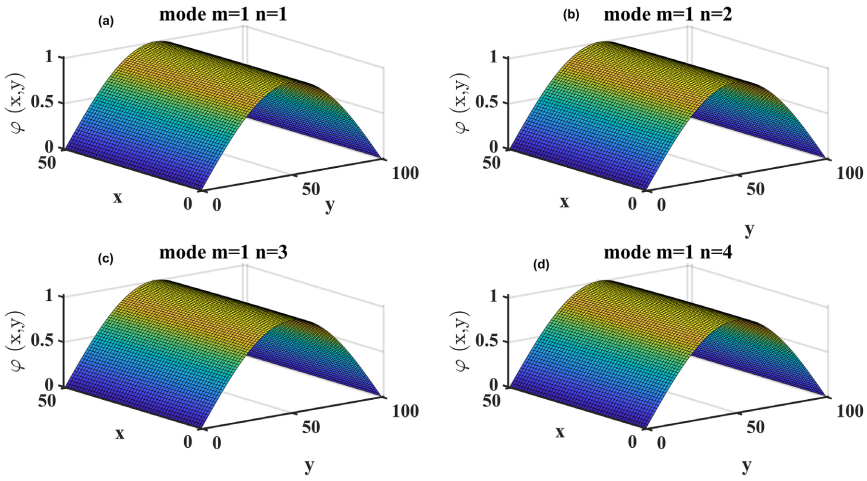

Figure 2. First mode in the y-direction and first to fourth modes in the x-direction. (a) mode (1, 1), (b) mode (1, 2), (c) mode (1, 3) and (d) mode (1, 4). The parameters used are obtained from **Equation (18)** and Table 1 and Table 2.

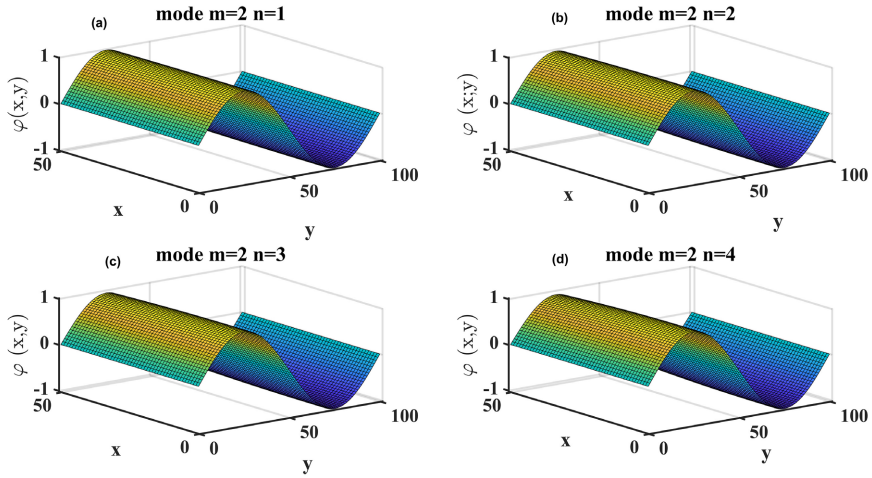

Figure 3. Second mode in the y-direction and first to fourth modes in the x-direction. (a) mode (2, 1), (b) mode (2, 2), (c) mode (2, 3) and (d) mode (2, 4). The parameters used are obtained from **Equation (18)** and Table 1 and Table 2.

Table 3. The first four natural frequencies of the thin rectangular plate.

Mode of vibration (*m*, *n*)	Natural frequency	Mode of vibration (*m*, *n*)	Natural frequency
(1, 1)	78.3621	(2, 1)	312.02
(1, 2)	79.194	(2, 2)	314.72
(1, 3)	80.2134	(2, 3)	317.17
(1, 4)	81.444	(2, 4)	321.16

Table 3 shows the natural frequency of each mode presented in Figure 3 and Figure 4 when the mode number is higher, its natural vibration frequency is higher. In the *y*-direction, the natural frequencies of the modes are close to each other. However, in the *x*-direction, the natural frequencies increase significantly. Thus, the mode with the smallest frequency is the mode (1, 1); therefore, the analysis is limited to the first mode, since the first mode of vibration is expected to carry most of the energy, and thus it should suffice to obtain a first estimate of the system behavior. The same analysis has been carried out by Jiao Jiang *et al.* [2]. Figure 4 shows the evolution of the energy delivered by the motor to make the plate vibrate as a function of the motor's supply voltage. We observe that the energy delivered by the motor increases linearly with the supply voltage when $u_1 \prec 20.4$ and when $u_1 \succ 20.6$. When $20.4 \le u_1 \le 20.6$, a nonlinear jump phenomenon appears; this indicates that the motor interacts significantly with the plate in this voltage range which is explained by the fact that the structure vibrates at a high amplitude.

Moreover, the average angular velocity also increases linearly with the supply voltage. However, within the same voltage range, a nonlinear jump phenomenon also occurs, reflecting the disturbance in the motor's operation caused by high-amplitude vibrations of the plate. It is clear that the non-ideal loading depends on the response of the structure. This jump phenomenon was also observed by Wenjie Li *et al.* [8] and was referred to as the Sommerfeld effect (circled zone in Figure 4).

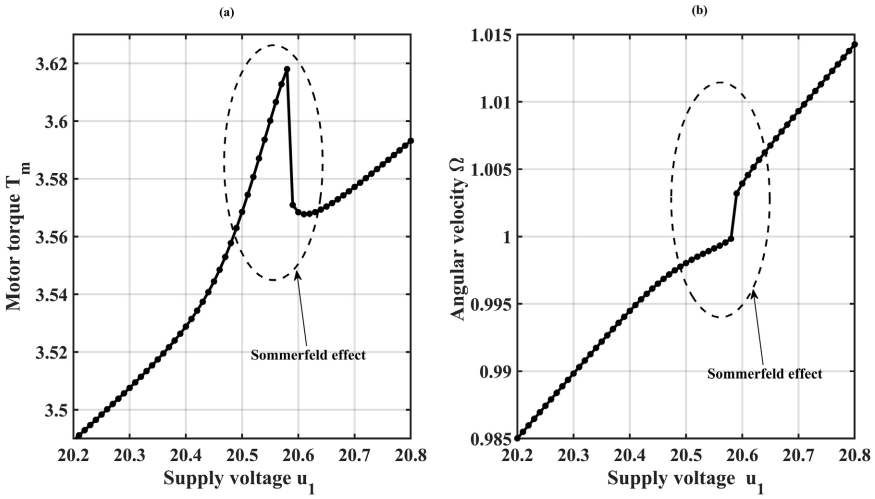

Figure 4. Steady state amplitude of (a) the motor torque and (b) the angular velocity versus the supply voltage. Appearance of the Sommerfeld effect. The parameters used are obtained from **Equation (18)** and Table 1 and Table 2.

The amplitude of oscillation of the plate is also evaluated and compared with numerical simulations obtained using the fourth-order Runge-Kutta method [19], as shown in Figure 5. The data reported in Figure 5 show the vibration amplitudes as a function of the supply voltage and as a function of angular speed. It is demon-

strated that as the supply voltage increases, the vibration amplitudes of the thin rectangular plate also increase, reaching a maximum value of 0.00092 at a voltage of 20.58. This voltage corresponds to the point at which the structure. vibrates with high amplitude. If the voltage is increased further, a considerable drop in the plate amplitude is observed, reflecting the strongly nonlinear effect of the voltage on the plate response, such as the occurrence of the Sommerfeld phenomenon in the system. The Sommerfeld phenomenon reflects the disturbance in the motor's operation due to high vibration amplitudes of the plate, or a significant interaction between the plate and the motor that affects the proper functioning of the latter.

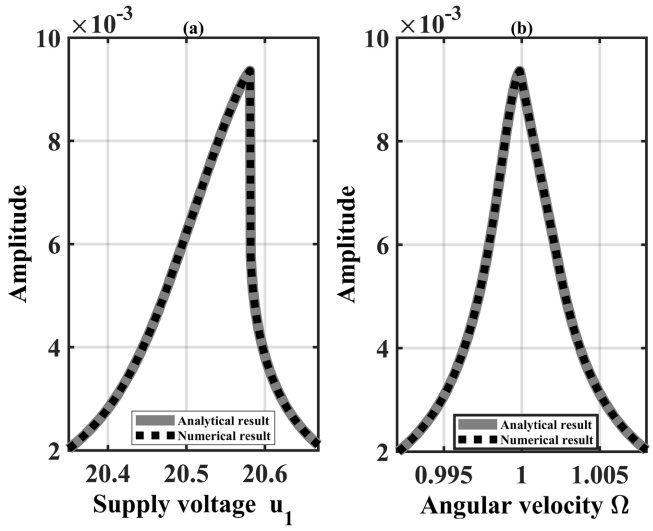

Figure 5. Steady state vibration amplitude of the plate as function of (a) a current voltage and (b) the average angular velocity. The dotted line represents the numerical results obtained by simulating the full **Equation (19a)**, while the solid curves are the analytical results from **Equation (20).** The parameters used are obtained from **Equation (18)** and Table 1 and Table 2.

Figure 6 shows the influence of the plate's damping coefficient on the occurrence of the Sommerfeld effect. It indicates that when the plate's damping coefficient is low, the interaction between the plate and the motor is stronger, as the structure does not dissipate enough of the energy transmitted by the motor.

According to Figure 7, for damping coefficients of 0.005 and 0.01, the amplitude jump does not appear and the structure vibrates with a low amplitude. Furthermore, when the damping coefficient is very small (0.0035), the amplitude jump appears, indicating the presence of the Sommerfeld effect, and the structure vibrates with a higher amplitude. Baltazar *et al.* [5] also obtained the same result in 2008.

Figure 8 shows the effect of the unbalanced mass on the steady-state amplitude of the rectangular plate. The resonance peak amplitude increases as the unbalanced mass m_0 increases. In short, the resonance of the plate strongly depends on the unbalanced mass. This observation indicates that a high value of this parameter can cause large displacements, thereby reducing the life expectancy of the plate. It is also observed that the resonance peak progressively shifts toward lower

supply voltage values as the unbalanced mass increases. This implies that for larger values of the unbalanced mass, the system reaches resonance more quickly, leading to a significant interaction between the motor and the structure, which disrupts the proper functioning of the motor. The shift of the peak amplitude also shows that a low-mass motor requires more electrical energy to make the structure vibrate compared to a high-mass motor. In other words, a low-mass motor must be sufficiently powerful to induce vibration in the structure.

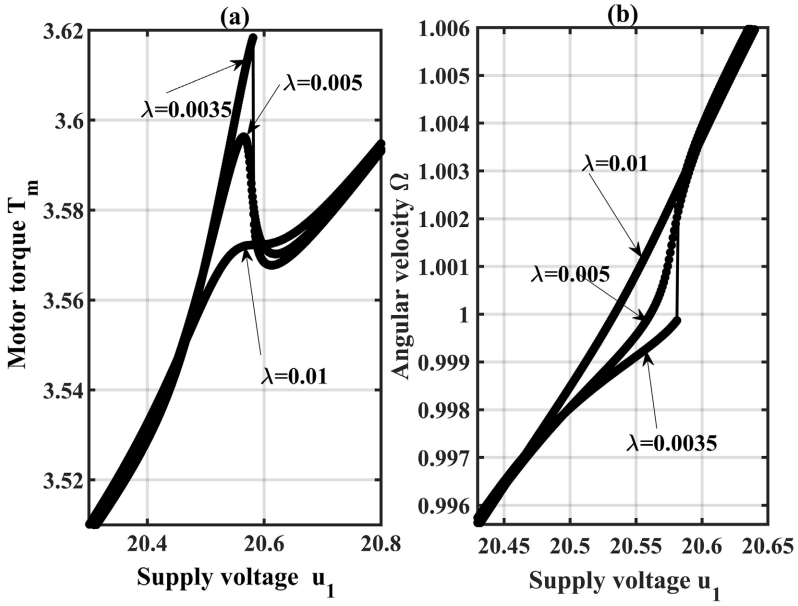

Figure 6. (a) Motor torque and (b) motor angular velocity as a function of voltage for different values of damping coefficient. The parameters used are obtained from **Equation (18)** and Table 1 and Table 2.

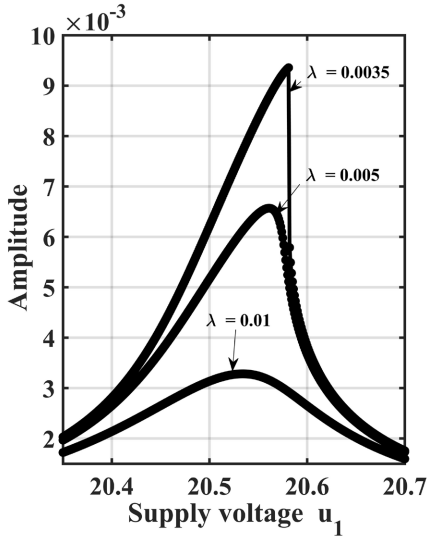

Figure 7. Vibration amplitude of the plate for different values of the plate damping coefficient. The parameters used are obtained from **Equation (18)** and Table 1 and Table 2.

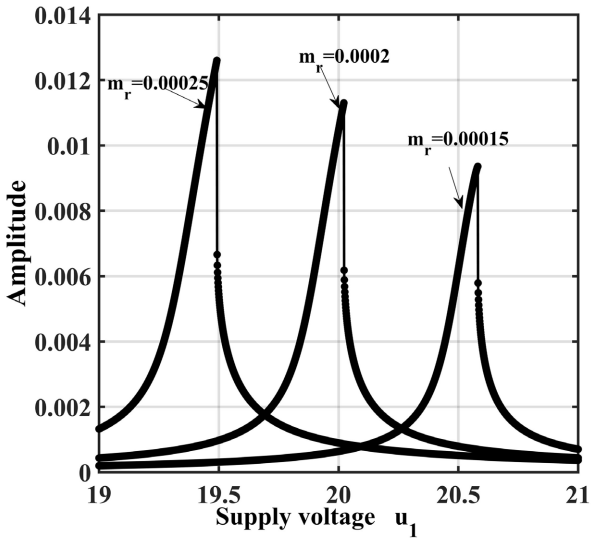

Figure 8. Effect of the unbalanced mass on the steady-state vibration amplitude of the rectangular plate. The parameters used are obtained from **Equation (18)** and Table 1 and Table 2.

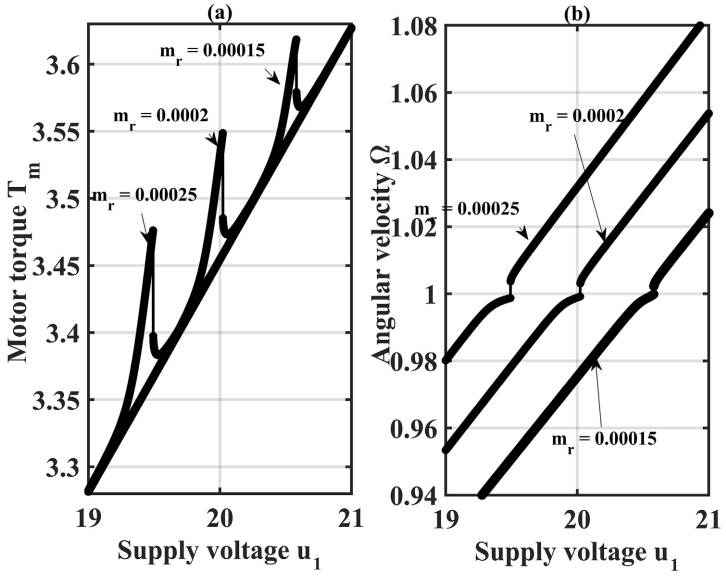

Figure 9. Effect of the unbalanced mass on (a) the motor torque and (b) the angular velocity for varying supply voltage**.** The parameters used are obtained from **Equation (18)** and Table 1 and Table 2.

Figure 8 shows the effect of the unbalanced mass on the steady-state amplitude of the rectangular plate. The resonance peak amplitude increases as the unbalanced mass m_0 increases. In short, the resonance of the plate strongly depends on the unbalanced mass. This observation indicates that a high value of this parameter can cause large displacements, thereby reducing the life expectancy of the plate. It is also observed that the resonance peak progressively shifts toward lower supply voltage values as the unbalanced mass increases. This implies that for larger values of the unbalanced mass, the system reaches resonance more quickly, lead-

ing to a significant interaction between the motor and the structure, which disrupts the proper functioning of the motor. The shift of the peak amplitude also shows that a low-mass motor requires more electrical energy to make the structure vibrate compared to a high-mass motor. In other words, a low-mass motor must be sufficiently powerful to induce vibration in the structure.

In Figure 9, we further demonstrate the influence of the unbalanced mass of the motor on the occurrence of the Sommerfeld phenomenon in the system, in terms of the energy delivered by the motor. It is observed that a motor with a low unbalanced mass interacts significantly with the structure for a given supply voltage; however, this interaction is less pronounced compared to motors with a high unbalanced mass. Furthermore, the angular velocity increases as the unbalanced mass increases. The observed jumps in energy and angular velocity become more pronounced as the mass increases. These significant jumps indicate that a motor with a large unbalanced mass is more disturbed than motors with lower mass and causes the structure to vibrate at a higher frequency. This is due to the fact that when the unbalanced mass is large, the plate vibrates with a greater amplitude, which in turn increases the displacement of the motor shaft.

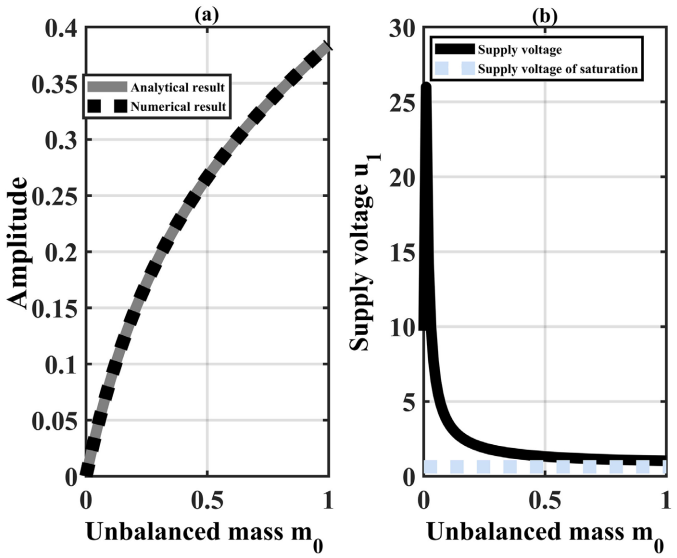

Figure 10. Evolution of (a) the steady-state amplitude and (b) the current voltage as a function of motor's mass. The dotted line represents the numerical results obtained by simulating the full **Equation (19a),** while the solid curves are the analytical results from **Equation (20).** The parameters used are obtained from **Equation (18)** and Table 1 and Table 2.

Figure 10 confirms that the vibration amplitudes increase with the mass of the motor. We also observe a non-monotonic relationship between the supply voltage and the motor's mass. In fact, as the mass increases, the supply voltage also increases, reaches a peak value, and thereafter decreases, eventually remaining constant around a limiting value $u_{1stat} = 0.63$. Thus, when the motor mass is significant, the load on the plate increases, and the motor becomes unable to make the plate vibrate because the required voltage is low. This phenomenon is called the

limited energy source phenomenon related to voltage saturation. Such an effect of the motor's mass has been extensively discussed in the context of non-ideal systems [1] [8]. For the investigated parameters, the numerical results are also found to be in good agreement with the analytical predictions.

4. Conclusions

Summing up, the strongly nonlinear effects of an unbalanced mass and the supply voltage of a non-ideal DC motor on the vibration amplitude of a thin rectangular plate have been investigated. The Lagrange formalism was used to establish the governing equations of the system. Subsequently, an averaging perturbation method was employed to obtain the steady-state response, and numerical simulations based on the fourth-order Runge-Kutta method were used to validate the analytical results. The influence of two main parameters—unbalanced mass and supply voltage of the DC motor—on the occurrence of the Sommerfeld phenomenon (in terms of the energy delivered by the motor) and on the appearance of the so-called limited energy source phenomenon related to voltage saturation has been thoroughly analyzed. The analysis leads us to the conclusion that the resonance peak of the plate amplitude increases as the unbalanced mass m_r increases. In short, the resonance of the plate strongly depends on the unbalanced mass. This indicates that a high value of this parameter can cause large displacements, thereby reducing the life expectancy of the plate. It is also observed that the resonance peak progressively shifts toward lower supply voltage values as the unbalanced mass increases, meaning that a low-mass motor requires more electrical energy to make the structure vibrate compared to a high-mass one. On the other hand, a non-monotonic behavior between the supply voltage and the motor's mass has been demonstrated. In fact, as the mass increases, the supply voltage also increases, reaches a peak value, and thereafter decreases, remaining constant around a limiting value $u_{1stat} = 0.63$. This phenomenon is referred to as the limited energy source phenomenon related to voltage saturation. Furthermore, the amplitude jump phenomenon, indicating the presence of the Sommerfeld effect, has been clearly captured by the analysis across a wide range of parameters. In industry, such phenomena can induce large vibrations of the plate and thereby contribute to structural failure and damage of the plate or the motor.

This exploratory analysis provides useful insights for the design of industrial floor structures supporting rotating machinery. It has, of course, its limitations. Most importantly, only the first mode was used in Galerkin's method, and higher coupled modes were not included. It would be interesting to extend this work to incorporate these higher modes; nevertheless, we hope that some qualitative conclusions obtained here can provide reference values for such developments.

Conflicts of Interest

The authors declare no conflicts of interest regarding the publication of this paper.

References

[1] Felix, J.L.P., Balthazar, J.M. and Brasil, R.M.L.R.F. (2005) On Saturation Control of a Non-Ideal Vibrating Portal Frame Foundation Type Shear-Building. *Journal of Vibration and Control*, **11**, 121-136. https://doi.org/10.1177/1077546305047656

[2] Jiang, J., Kong, X., Chen, C. and Zhang, Z. (2021) Dynamic and Stability Analysis of a Cantilever Beam System Excited by a Non-Ideal Induction Motor. *Meccanica*, **56**, 1675-1691. https://doi.org/10.1007/s11012-021-01333-3

[3] Samantaray, A.K., Dasgupta, S.S. and Bhattacharyya, R. (2010) Sommerfeld Effect in Rotationally Symmetric Planar Dynamical Systems. *International Journal of Engineering Science*, **48**, 21-36. https://doi.org/10.1016/j.ijengsci.2009.06.005

[4] Felix, J.L.P., Balthazar, J.M. and Brasil, R.M.L.R.F. (2009) Comments on Nonlinear Dynamics of a Non-Ideal Duffing-Rayleigh Oscillator: Numerical and Analytical Approaches. *Journal of Sound and Vibration*, **319**, 1136-1149. https://doi.org/10.1016/j.jsv.2008.06.036

[5] Balthazar, J.M., *et al.* (2025) A State of the Art on Recent Progress and Emerging Challenges on Energy Transfer Between Vibrating Modes Under an External Mechanical Force with Time-Varying Frequency From 2020 to 2025. arXiv: 2506.01469.

[6] Kovriguine, D.A. (2011) Synchronization and Sommerfeld Effect as Typical Resonant Patterns. *Archive of Applied Mechanics*, **82**, 591-604. https://doi.org/10.1007/s00419-011-0574-4

[7] Kong, X., Jiang, J., Zhou, C., Xu, Q. and Chen, C. (2020) Sommerfeld Effect and Synchronization Analysis in a Simply Supported Beam System Excited by Two Non-Ideal Induction Motors. *Nonlinear Dynamics*, **100**, 2047-2070. https://doi.org/10.1007/s11071-020-05626-2

[8] Li, W., Kong, X., Xu, Q., Zhou, C. and Hao, Z. (2023) Nonlinear Dynamic Response of a Thin Rectangular Plate Vibration System Excited by a Non-Ideal Induction Motor. *Journal of Vibration Engineering & Technologies*, **11**, 1211-1227. https://doi.org/10.1007/s42417-022-00637-2

[9] Kong, X., Zeng, F., Kong, F. and Wu, T. (2024) Dynamic Stability of Thin Rectangular Plates Subjected to Excitations Provided by Three Vibrators. *Nonlinear Dynamics*, **112**, 18949-18975. https://doi.org/10.1007/s11071-024-10035-w

[10] Gonçalves, P.J.P., Silvera, M. and Pontes, B.R. (2014) Numerical and Experimental Investigation of a Vibration System with Non-Ideal Vibration Source. *Proceedings of the* 9*th International Conference on Structural Dynamics*, Portugal, 30 June-2 July 2014, 2113-2117.

[11] Nzengwa, R. (2025) Plate and Shell Models. Springer.

[12] Timoshenko, S.P. (1959) Theory of Plates and Shells. Wiley.

[13] Feulefack Songong, E., Nanha Djanan, A.A. and Nana Nbendjo, B.R. (2021) Vibration Absorption of a Rectangular Plate Supporting a DC Motor with a TLCD. *Springer Nature*, **105**, 1357-1327. https://doi.org/10.1007/s11071-021-06671-1

[14] Djanan, A.N., Nbendjo, B.N. and Woafo, P. (2015) Self-Synchronization of Two Motors on a Rectangular Plate and Reduction of Vibration. *Journal of Vibration and Control*, **21**, 2114-2123. https://doi.org/10.1177/1077546313506925

[15] Yildiz, A.B. (2012) Electrical Equivalent Circuit Based Modeling and Analysis of Direct Current Motors. *International Journal of Electrical Power & Energy Systems*, **43**, 1043-1047. https://doi.org/10.1016/j.ijepes.2012.06.063

[16] Soedel, W. (2005) Vibrations of Shells and Plates. Taylor Francis

[17] Nanha Djanan, A.A., Nana Nbendjo, B.R. and Woafo, P. (2013) Electromechanical Control of Vibration on a Plate Submitted to a Non-Ideal Excitation. *Mechanics Research Communications*, **54**, 72-82. https://doi.org/10.1016/j.mechrescom.2013.09.012

[18] Bouna, H.S. and Nbendjo, B.R.N. (2012) Vibration Control of a Plate Subjected to Impulsive Force by Plate-Type Dynamic Vibration Absorbers. *World Journal of Mechanics*, **2**, 143-151. https://doi.org/10.4236/wjm.2012.23017

[19] Tabejieu, L.M.A., Nbendjo, B.R.N., Filatrella, G. and Woafo, P. (2017) Amplitude Stochastic Response of Rayleigh Beams to Randomly Moving Loads. *Nonlinear Dynamics*, **89**, 925-937. https://doi.org/10.1007/s11071-017-3492-3

Appendix

Appendix 1: Evaluation of the Mode Shape Function and the Natural Frequency of the Plate Vibration

Let us consider the governing equation of plate (**Equation (7a)** of the main document), without damping and excitation:

$$\rho h\frac{\partial^2 w}{\partial t^2}+D\left(\frac{\partial^4 w}{\partial x^4}+\frac{\partial^4 w}{\partial y^4}+2\frac{\partial^4 w}{\partial x^2\partial y^2}\right)=0 \tag{A1.1}$$

The solution of **Equation (A1.1)** is obtained by using the method of the variable separation. Thus,

$$w(x,y,t)=\sum_{n=1}^{\infty}\sum_{m=1}^{\infty}q_{nm}(t)\varphi_{nm}(x,y) \tag{A1.2}$$

By substituting **Equation (A1.2)** into **Equation (A1.1)**, the eigenvalues equation of the system is given by:

$$\nabla^4\varphi_{nm}(x,y)-\frac{\omega_{nm}^2\rho h\varphi_{nm}(x,y)}{D}=0 \tag{A1.3}$$

According to the boundary conditions (simply supported edges in y-axis direction and free edges in the x-axis direction), the mode shape function $\varphi_{nm}(x,y)$ is given as [8]:

$$\varphi_{nm}(x,y)=X_n(x)\sin\left(\frac{m\pi y}{b}\right) \tag{A1.4}$$

where m is the number of half-waves in the y-axis direction; n is the number of half-waves in the x-axis direction.

Substituting **Equation (A1.4)** into **Equation (A1.3)**, we can obtain

$$X_n^{(4)}(x)-2\left(\frac{m\pi}{b}\right)^2X_n^{(2)}(x)+\left(\left(\frac{m\pi}{b}\right)^4-\beta_{nm}^4\right)X_n(x)=0 \tag{A1.5}$$

where $\beta_{nm}^4=\dfrac{\rho h\omega_{nm}^2}{D}$.

The characteristic equation of **Equation (A1.5)** is given by:

$$r^4-2\left(\frac{m\pi}{b}\right)^2r^2+\left(\left(\frac{m\pi}{b}\right)^4-\beta_{nm}^4\right)=0 \tag{A1.6}$$

The solutions of **Equation (A1.6)** are given by:

$$\begin{cases} r=j\alpha_n; & r=-j\alpha_n \\ r=\tau_n; & r=-\tau_n \\ j^2=-1 \end{cases} \quad \text{with} \quad \begin{cases} \alpha_n=\sqrt{\beta_{nm}^2-\left(\dfrac{m\pi}{b}\right)^2} \\ \tau_n=\sqrt{\left(\dfrac{m\pi}{b}\right)^2+\beta_{nm}^2} \\ \omega_{nm}=\beta_{nm}^2\sqrt{\dfrac{D}{\rho h}}=\dfrac{\alpha_n^2+\tau_n^2}{2}\sqrt{\dfrac{D}{\rho h}} \end{cases} \tag{A1.7}$$

The general solution of **Equation (A1.5)** is given by:

$$X_n(x) = A_n \cos(\alpha_n x) + B_n \sin(\alpha_n x) + C_n ch(\tau_n x) + D_n sh(\tau_n x) \tag{A1.8}$$

By applying the boundary conditions given by **(Equation (10) of the main document)**. we obtain the following homogeneous linear system:

$$\begin{cases} \alpha_n B_n + \tau_n D_n = 0 \\ -\alpha_n^2 A_n + \tau_n^2 C_n = 0 \\ -\alpha_n A_n \sin(\alpha_n a) + \alpha_n B_n \cos(\alpha_n a) + \tau_n C_n sh(\tau_n a) + \tau_n D_n ch(\tau_n a) = 0 \\ -\alpha_n^2 A_n \cos(\alpha_n a) - \alpha_n^2 B_n \sin(\alpha_n a) + \tau_n^2 C_n ch(\tau_n a) + \tau_n^2 D_n sh(\tau_n a) = 0 \end{cases} \tag{A1.9}$$

Since A_n, B_n, C_n, D_n cannot be zero at the same time, the coefficient determinant of **Equation (A1.7)** is zero:

$$\begin{vmatrix} 0 & \alpha_n & 0 & \tau_n \\ -\alpha_n^2 & 0 & \tau_n^2 & 0 \\ -\alpha_n \sin(\alpha_n a) & \alpha_n \cos(\alpha_n a) & \tau_n sh(\tau_n a) & \tau_n ch(\tau_n a) \\ -\alpha_n^2 \cos(\alpha_n a) & -\alpha_n^2 \sin(\alpha_n a) & \tau_n^2 ch(\tau_n a) & \tau_n^2 sh(\tau_n a) \end{vmatrix} = 0 \tag{A1.10}$$

By expanding and simplifying **Equation (A1.8),** the transcendental equation for the natural frequency can be obtained as follows:

$$\left(\alpha_n^2 - \tau_n^2\right) sh(\tau_n a) \sin(\alpha_n a) + 2\alpha_n \tau_n \left(ch(\tau_n a)\cos(\alpha_n a) - 1\right) = 0 \tag{A1.11}$$

$$\text{For: } A_n = 1; C_n = \left(\frac{\alpha_n}{\tau_n}\right)^2; D_n = -\frac{\alpha_n}{\tau_n} B_n; B_n = \frac{ch(\tau_n a) - \cos(\alpha_n a)}{\sin(\alpha_n a) + \frac{\tau_n}{\alpha_n} sh(\tau_n a)} \tag{A1.12}$$

Finally, by substituting all the previous coefficients, we obtain the expression of the vibration mode shape given by:

$$\varphi_{nm}(x,y) = \left(\cos(\alpha_n x) + \left(\frac{\alpha_n}{\tau_n}\right)^2 ch(\tau_n x) + \frac{ch(\tau_n a) - \cos(\alpha_n a)}{\sin(\alpha_n a) + \frac{\tau_n}{\alpha_n} sh(\tau_n a)} \left(\sin(\alpha_n x) - \frac{\alpha_n}{\tau_n} sh(\tau_n x) \right) \right) \sin\left(\frac{m\pi y}{b}\right) \tag{A1.13}$$

Appendix 2: Calculation of the Integrals of Equation (13) in the Main Document

Equation (13) of the document is rewritten as follows:

$$\begin{aligned} &M_{nm} = \left(\rho h + \frac{m_0}{ab}\right) \int_0^a \int_0^b \varphi_{nm}^2(x,y)\,dx\,dy;\ \lambda_{nm} = \lambda h \int_0^a \int_0^b \varphi_{nm}^2(x,y)\,dx\,dy; \\ &K_{nm} = D \int_0^a \int_0^b \varphi_{nm}(x,y) \left(\frac{\partial^4 \varphi_{nm}(x,y)}{\partial x^4} + \frac{\partial^4 \varphi_{nm}(x,y)}{\partial y^4} + 2\frac{\partial^4 \varphi_{nm}(x,y)}{\partial x^2 \partial y^2} \right) dx\,dy; \\ &f_{nm} = \int_0^a \int_0^b \varphi_{nm}(x,y) \left[H(x - x_0) - H(x - x_0') \right] \times \left[H(y - y_0) - H(y - y_0') \right] dx\,dy; \\ &T_{nm} = \int_0^a \int_0^b \varphi_{nm}(x,y)\,dx\,dy;\ L_{nm} = \int_0^a \int_0^b \varphi_{nm}^2(x,y)\,dx\,dy. \end{aligned} \tag{A2.1}$$

The vibration mode shapes the plate $\varphi_{nm}(x,y)$ is demonstrated previously and given by **Equation (A1.11)**. After substituting this equation **(Equation (A1.11))**. into **Equation (A2.1)**, using Table of Integrals, expanding and simplifying the expression obtained, the coefficients $M_{nm}, K_{nm}, \lambda_{nm}, f_{nm}, T_{nm}, L_{nm}$ are evaluated and given by:

$$\begin{aligned} M_{nm} &= \left(\rho h + \frac{m_0}{ab}\right)\int_0^a\int_0^b \varphi_{nm}^2(x,y)\,\mathrm{d}x\,\mathrm{d}y \\ &= \frac{b}{2}\left(\rho h + \frac{m_0}{ab}\right)\left(\frac{a}{2}\left(1+\kappa_n^2+t_n^2\left(t_n^2-\kappa_n^2\right)\right)+\frac{1}{4\alpha_n}\left(1-\kappa_n^2\right)\sin\left(2\alpha_n a\right)\right. \\ &\quad + \frac{t_n^2}{4\tau_n}\left(1+\kappa_n^2\right)sh\left(2\tau_n a\right)+\frac{2t_n^2}{\tau_n\left(1+t_n^2\right)}\left(1+\kappa_n^2\right)sh\left(\tau_n a\right)\cos\left(\alpha_n a\right) \\ &\quad + \frac{2t_n}{\tau_n\left(1+t_n^2\right)}\left(t_n^2-\kappa_n^2\right)ch\left(\tau_n a\right)\sin\left(\alpha_n a\right)-\frac{\kappa_n}{\alpha_n}\left(\cos\left(2\alpha_n a\right)-1\right) \\ &\quad \left. + \frac{\kappa_n t_n^3}{\tau_n}\left(ch\left(2\tau_n a\right)-1\right)+\frac{2\kappa_n t_n}{\tau_n}\left(1-\cos\left(\alpha_n a\right)ch\left(\tau_n a\right)\right)\right) \end{aligned} \tag{A2.2}$$

$$\begin{aligned} K_{nm} &= D\int_0^a\int_0^b \varphi_{nm}(x,y)\left(\frac{\partial^4\varphi_{nm}(x,y)}{\partial x^4}+\frac{\partial^4\varphi_{nm}(x,y)}{\partial y^4}+2\frac{\partial^4\varphi_{nm}(x,y)}{\partial x^2\partial y^2}\right)\mathrm{d}x\,\mathrm{d}y \\ &= \frac{bD}{2}\left(P_{nm}+\frac{1}{4\alpha_n}\sin\left(2\alpha_n a\right)\left(A_{nm}-\kappa_n C_{nm}\right)+\frac{1}{4\tau_n}sh\left(2\tau_n a\right)\left(t_n^2 B_{nm}-D_{nm}t_n\kappa_n\right)\right. \\ &\quad \left. - S_{nm}\left(\cos\left(2\alpha_n a\right)-1\right)+U_{nm}\left(ch\left(2\tau_n a\right)-1\right)+\frac{1}{\tau_n\left(1+t_n^2\right)}G_{nm}+\frac{1}{\tau_n\left(1+t_n^2\right)}H_{nm}\right) \end{aligned} \tag{A2.3}$$

$$\begin{aligned} \lambda_{nm} &= \lambda h\int_0^a\int_0^b \varphi_{nm}^2(x,y)\,\mathrm{d}x\,\mathrm{d}y \\ &= \frac{bC}{2}\left(\frac{a}{2}\left(1+\kappa_n^2+t_n^2\left(t_n^2-\kappa_n^2\right)\right)+\frac{1}{4\alpha_n}\left(1-\kappa_n^2\right)\sin\left(2\alpha_n a\right)+\frac{t_n^2}{4\tau_n}\left(1+\kappa_n^2\right)sh\left(2\tau_n a\right)\right. \\ &\quad + \frac{2t_n^2}{\tau_n\left(1+t_n^2\right)}\left(1+\kappa_n^2\right)sh\left(\tau_n a\right)\cos\left(\alpha_n a\right)+\frac{2t_n}{\tau_n\left(1+t_n^2\right)}\left(t_n^2-\kappa_n^2\right)ch\left(\tau_n a\right)\sin\left(\alpha_n a\right) \\ &\quad \left. - \frac{\kappa_n}{\alpha_n}\left(\cos\left(2\alpha_n a\right)-1\right)+\frac{\kappa_n t_n^3}{\tau_n}\left(ch\left(2\tau_n a\right)-1\right)+\frac{2\kappa_n t_n}{\tau_n}\left(1-\cos\left(\alpha_n a\right)ch\left(\tau_n a\right)\right)\right) \end{aligned} \tag{A2.4}$$

$$\begin{aligned} f_{nm} &= \int_0^a\int_0^b \varphi_{nm}(x,y)\left[H\left(x-x_0\right)-H\left(x-x_0'\right)\right]\times\left[H\left(y-y_0\right)-H\left(y-y_0'\right)\right]\mathrm{d}x\,\mathrm{d}y \\ &= \frac{b}{m\pi}\left(\frac{1}{\alpha_n}\left(\sin\left(\alpha_n x_0'\right)-\sin\left(\alpha_n x_0\right)\right)+\frac{t_n^2}{\tau_n}\left(sh\left(\tau_n x_0'\right)-sh\left(\tau_n x_0\right)\right)\right. \\ &\quad \left. + \frac{\kappa_n}{\alpha_n}\left(\cos\left(\alpha_n x_0\right)-\cos\left(\alpha_n x_0'\right)\right)+\frac{\kappa_n t_n}{\tau_n}\left(ch\left(\tau_n x_0\right)-ch\left(\tau_n x_0'\right)\right)\right) \\ &\quad \times\left(\cos\left(\frac{m\pi y_0}{b}\right)-\cos\left(\frac{m\pi y_0'}{b}\right)\right) \end{aligned} \tag{A2.5}$$

$$T_{nm}=\int_0^a\int_0^b \varphi_{nm}(x,y)\,\mathrm{d}x\,\mathrm{d}y$$
$$=-\frac{b}{m\pi}\left(\cos(m\pi)-1\right)\left(\frac{1}{\alpha_n}\sin(\alpha_n a)+\frac{t_n^2}{\tau_n}sh(\tau_n a)\right. \tag{A2.6}$$
$$\left.-\kappa_n\left(\frac{1}{\alpha_n}\left(\cos(\alpha_n a)-1\right)+\frac{t_n}{\tau_n}\left(ch(\tau_n a)-1\right)\right)\right)$$

$$L_{nm}=\int_0^a\int_0^b \varphi_{nm}^2(x,y)\,\mathrm{d}x\,\mathrm{d}y$$
$$=\frac{b}{2}\left(\frac{a}{2}\left(1+\kappa_n^2+t_n^2\left(t_n^2-\kappa_n^2\right)\right)+\frac{1}{4\alpha_n}\left(1-\kappa_n^2\right)\sin(2\alpha_n a)+\frac{t_n^2}{4\tau_n}\left(1+\kappa_n^2\right)sh(2\tau_n a)\right.$$
$$+\frac{2t_n^2}{\tau_n\left(1+t_n^2\right)}\left(1+\kappa_n^2\right)sh(\tau_n a)\cos(\alpha_n a)+\frac{2t_n}{\tau_n\left(1+t_n^2\right)}\left(t_n^2-\kappa_n^2\right)ch(\tau_n a)\sin(\alpha_n a) \tag{A2.7}$$
$$\left.-\frac{\kappa_n}{\alpha_n}\left(\cos(2\alpha_n a)-1\right)+\frac{\kappa_n t_n^3}{\tau_n}\left(ch(2\tau_n a)-1\right)+\frac{2\kappa_n t_n}{\tau_n}\left(1-\cos(\alpha_n a)ch(\tau_n a)\right)\right)$$

where:

$$t_n=\frac{\alpha_n}{\tau_n};\ A_{nm}=\alpha_n^4+\left(\frac{m\pi}{b}\right)^4+2\left(\frac{\alpha_n m\pi}{b}\right)^2;$$
$$B_{nm}=\left(\alpha_n\tau_n\right)^2+t_n^2\left(\frac{m\pi}{b}\right)^4-2\left(\alpha_n\right)^2\left(\frac{m\pi}{b}\right)^2;$$
$$C_{nm}=\kappa_n\left(2\alpha_n^2\left(\frac{m\pi}{b}\right)^2+\alpha_n^4+\left(\frac{m\pi}{b}\right)^4\right);$$
$$D_{nm}=-\kappa_n\left(\alpha_n\left(\tau_n\right)^3+\left(\frac{m\pi}{b}\right)^4 t_n-2\alpha_n\tau_n\left(\frac{m\pi}{b}\right)^2\right);$$
$$S_{nm}=\frac{C_{nm}+\kappa_n A_{nm}}{4\alpha_n};\ U_{nm}=\frac{t_n^2 D_{nm}-B_{nm}t_n\kappa_n}{4\tau_n};$$
$$P_{nm}=\frac{a}{2}\left(A_{nm}+\kappa_n C_{nm}+t_n^2 B_{nm}+D_{nm}t_n\kappa_n\right);$$
$$G_{nm}=\left(D_{nm}-A_{nm}t_n\kappa_n-t_n\left(t_n^2 C_{nm}+\kappa_n B_{nm}\right)\right)\cos(\alpha_n a)ch(\tau_n a)$$
$$+\left(t_n\left(D_{nm}-A_{nm}t_n\kappa_n\right)+t_n^2 C_{nm}+\kappa_n B_{nm}\right)sh(\tau_n a)\sin(\alpha_n a);$$
$$H_{nm}=\left(t_n^2 A_{nm}+B_{nm}-t_n\left(D_{nm}\kappa_n-C_{nm}t_n\kappa_n\right)\right)sh(\tau_n a)\cos(\alpha_n a)$$
$$+\left(t_n\left(t_n^2 A_{nm}+B_{nm}\right)+D_{nm}\kappa_n-C_{nm}t_n\kappa_n\right)ch(\tau_n a)\sin(\alpha_n a) \tag{A2.8}$$